— 11 —

UV Radiometric Calibration of UVCS

LARRY D. GARDNER, PETER L. SMITH, JOHN L. KOHL,
NIGEL ATKINS, ANGELA CIARAVELLA, MARI PAZ MIRALLES,
ALEXANDER PANASYUK, JOHN C. RAYMOND,
LEONARD STRACHAN, JR., RAID M. SULEIMAN

Harvard-Smithsonian Center for Astrophysics, Cambridge, MA, USA

MARCO ROMOLI

Univ. di Firenze, Firenze, Italy

SILVANO FINESCHI

Osservatorio Astronomico di Torino, Pino Torinese, Italy

The Ultraviolet Coronagraph Spectrometer (UVCS) was characterized and radiometrically calibrated in the laboratory as a system at the Harvard-Smithsonian Center for Astrophysics in June of 1995. Component level calibrations of optical components and detectors were also performed. After launch, an in-flight calibration activity was carried out that extended the laboratory calibration, compared UVCS measurements of stars to those of other instruments and monitored the radiometric stability of UVCS through repeated measurements of stars that are believed to have nearly constant ultraviolet irradiance. In-flight measurements have, in general, confirmed the laboratory radiometric calibration. Comparisons to Spartan 201 observations of the same coronal structures agree within 10 %. The system responsivity, although it has changed somewhat during the six years of operation, is well behaved and characterizable. This paper describes the UVCS calibration and its results.

11.1 Introduction

In this paper we describe the radiometric calibration of UVCS and the current state of knowledge regarding its responsivity. This paper does not describe the extensive characterization of the instrument mechanisms and non-radiometric system properties that have been achieved through both laboratory and in-flight procedures. For example, the characterization of the variable slit widths is not presented even though this information is an integral part of the spectral radiance calibration. Similarly, the characterization of the pointing of the telescope mirrors is not described nor are the determinations of the wavelength scales and grating rotations. The laboratory characterization of the internal occulter position, which determines the limiting aperture for observations at selected heliographic heights, is not described, but the determination of the vignetting function, which depends on both the internal occulter position and variations of reflectances and grating efficiencies across the surface of the optical components, is described. Another important aspect

of the UVCS characterization is the stray light determination, which is a consideration for all UVCS observations. The stray light depends on the heliographic height of an observation. It can be determined by observing spectral lines of low charge state ions that do not exist in significant amounts in the corona. Comparisons of such measurements to laboratory stray light measurements yield consistent results. Calibration files containing all of this information as well as the radiometric calibration itself are included in the UVCS Data Analysis Software, which is available through the SOHO Archive and elsewhere. An important aspect of the in-flight calibration activity has been the monitoring of the detector gain stability. The gain of the microchannel plate (MCP) z-stack in the crossed-delay-line (XDL) detectors [*Siegmund et al.*, 1994] of UVCS degrades with accumulated photon dose on the photosensitive areas of the first MCP. This effect is believed to be a result of wear to the final MCP in the stack. In-flight measurements have been used to track the changes in gain across the detector surface and increase high voltage as necessary to ensure that the detected quantum efficiency remains constant to within ± 5 %.

The UVCS radiometric calibration is based on the pre-launch system level calibration, component calibrations and in-flight calibrations. The calibration of the O VI channel presented herein, including specified changes, is applicable for the entire mission. The calibration of the Ly-α channel is applicable through 3 September 1997 when the detector high voltage for that channel was lowered to reduce the current, and certain regions of the detector became unreliable. The system level laboratory calibration could only be done at one position of the internal occulter (i.e., the aperture used for observations at 2.7 solar radii). The in-flight calibration together with the component calibrations were used to extend the system calibration to all instrument apertures that have been used during the mission (i.e., those for every heliographic height observed). In-flight intercalibrations to UVCS/Spartan 201 and SUMER were accomplished using co-registered observations of the Sun during the mission. In addition, periodic measurements of stars, which are believed to have relatively constant UV spectral irradiances, have been used to determine the consistency of the UVCS calibration and that of Voyager, the International Ultraviolet Explorer (IUE) and Far Ultraviolet Spectroscopic Explorer (FUSE) spacecraft. Periodic measurements of the same stars have been used to indicate the stability of the UVCS responsivity over a six year period.

In-flight observations were also used to compare the laboratory radiometric calibrations of UVCS's two UV channels at overlapping wavelengths near 121.6 nm. A small difference was discovered. As a result, the calibrations of both channels were shifted so as to bring them into agreement with each other.

11.2 Instrument Description

The UVCS (see Figure11.1), a system of three externally and internally occulted telescopes feeding two ultraviolet spectrographic channels and one visible light polarimetric channel, has been described previously [*Kohl et al.*, 1995]. Light from the solar disk enters the UVCS aperture and is absorbed in a light trap mounted near the rear of the instrument. One edge of the aperture is a linear serrated blade that forms the edge of the external occulter; each UV telescope mirror resides in the shadow behind that occulter. Rays from the solar disk, diffracted by the external occulter, which would otherwise be specularly reflected by the telescope mirrors into the spectrograph, are intercepted by the internal

occulter which can move perpendicularly to the external occulter edge. The selected position of the internal occulter depends on the heliocentric height observed. In this way the limiting aperture of UVCS for any given observation is determined by the position of the internal occulter. The UV telescope optical surfaces themselves are chemical vapor deposited (CVD) silicon carbide on silicon carbide substrates. The mirrors have a spherical figure with 750 mm focal lengths. Both UV spectrographic channels are normal incidence Rowland circle designs. Both have adjustable entrance slits. The diffraction gratings are toric in figure [*Huber et al.*, 1988] with 750 mm major radii of curvature and are held in independently adjustable Johnson-Onaka style mechanisms. The detector systems are microchannel plate based with XDL anodes. The grating ranges and rulings are chosen so as to center the H I Ly-α line (121.6 nm) in one channel and the O VI doublet 103.2 and 103.7 nm in the other. Inside the O VI channel there is an auxiliary mirror that is strategically placed to divert a band of light which includes the H I Ly-α wavelength toward the O VI detector when the O VI grating is rotated to a specific range of angles. In this way a "redundancy" has been created for the portion of the spectrum containing H I Ly-α.

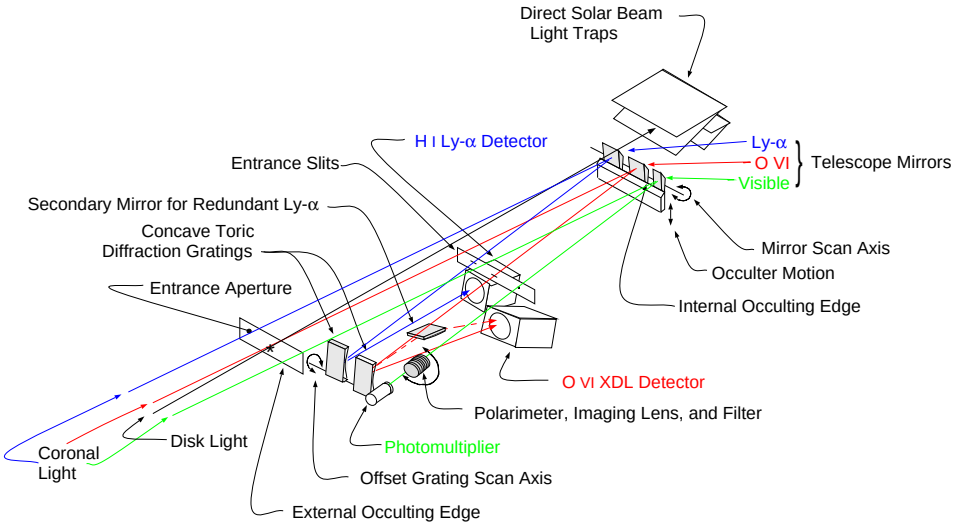

Figure 11.1: Schematic of the UVCS optical system.

The instantaneous field of view of UVCS is a variable width slice of the corona approximately $40'$ long (i.e., in the direction that is tangent to the disk). The width of the slice (i.e., in the radial direction) is given by the ratio of the spectrometer slit width to telescope focal length and so is selectable between about $1''$ and $1.4'$. The images recorded by the XDL detectors display spatial imaging information along the slit length and spectral information in the direction of the width. The UVCS can be rolled about the sun-center axis by approximately 350 degrees, and the telescope mirrors can be rotated from 1.2 to 10 $R_\odot$. UVCS can also change its normally sun-centered pointing by $\pm 35'$. In this way UVCS can observe radial heights from –1 to 12 $R_\odot$.

11.3 Cleanliness

Cleanliness was an issue of major concern during the fabrication, integration, and testing of UVCS. Its stray light performance is sensitive to light scattering by particulate contamination, and its optical efficiencies are affected by molecular contamination photopolymerized on its optical surfaces. While the former is routinely controlled by carrying out the work on the instrument in suitable conventional cleanrooms, the latter requires attention to all manner of details ranging from choices of construction materials to appropriate filtration through activated carbon of the air circulated in the aforementioned cleanrooms. For UVCS the cleanliness program was laid out in appropriate process control documents that specified a total allowable quantity of chemical and particulate surface contamination, procedures for cleaning parts allowable solvents and materials, etc. Since the structure of UVCS was constructed of graphite fiber reinforced epoxy (GFRE), which is sensitive to the absorption of moisture, it was also essential to control humidity and to keep the instrument purged with dry gas whenever it was not actively being assembled or tested. A rigorous program was set up to monitor the contaminant levels, including moisture absorption, throughout all stages of construction, integration, and testing in order to verify compliance with the control documents and to be able to take corrective action before levels approach the allowable limits. The program was reasonably successful overall, and certainly none of its rigor should be relaxed for any future instrument. However with the benefit of hindsight, some changes would be made, i.e., the allowance of additional time for optical testing and component change-out as necessary, and the addition of doors and active pumping to the detectors to prevent deterioration of the photocathodes. For further details of the UVCS cleanliness program, see *Schühle et al.* [2002].

11.4 Laboratory Measurements of Instrument Properties

The UVCS system level tests were carried out in laboratories at the Harvard-Smithsonian Center for Astrophysics in June of 1995. A description of that work was published in 1996 [*Gardner et al.,* 1996] and only will be summarized here. Owing to the design of the internal occulter mechanism, the UVCS system level calibrations were limited to one optical aperture – the one used for measurements at a heliocentric height of 2.7 $R_\odot$ and corresponding to the internal occulter's launch-locked position.

The count rate of the UVCS response to a source of spectral radiance I(λ) is:

$$C = (w_s h_s w_m h_m)/f^2 \int I(\lambda)\varepsilon(\lambda)d\lambda, \tag{11.1}$$

where w_s is the slit width, h_s is the slit height, w_m is the unvignetted mirror width, h_m is the mirror height and f is the telescope focal length. The system responsivity is given by:

$$\varepsilon(\lambda) = R_t(\lambda, x_t, y_t)E_g(\lambda, x_g, y_g)E_d(\lambda, x_d, y_d), \tag{11.2}$$

where $R_t(\lambda, x_t, y_t)$ is the mirror reflectance, $E_g(\lambda, x_g, y_g)$ is the grating efficiency including the coating and $E_d(\lambda, x_d, y_d)$ is the detected quantum efficiency of the detector system. All three of these quantities depend on wavelength and can vary over their respective surfaces. Hence, Equation (11.1) describes the count rate for a particular region of the aperture and a particular pixel.

The effective area for a particular wavelength λ_i is given by

$$A_{eff} = (w_m h_m)\varepsilon(\lambda_i), \tag{11.3}$$

where an average value over the aperture is used for R_t and E_g, and a reference area on the detector is used for E_d. Equations (11.1) and (11.3) are applicable to the primary Ly-α and direct O VI channels but not to the redundant Ly-α path, which contains an additional optic inside the spectrometer. See Section 11.5.3.

The general arrangement for the UVCS radiometric calibration is shown in Figure 11.2. Radiation from a gas discharge light source was predispersed using a 1 meter radius

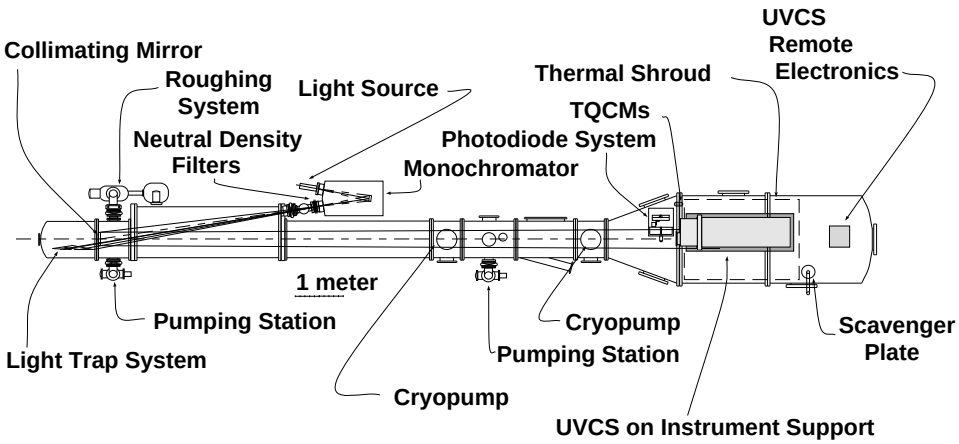

Figure 11.2: The arrangement for the UVCS system level calibration and characterization. This primary vacuum chamber and its peripheral units included the light sources, predispersing monochromator, the collimating mirror, standard photodiodes and instrument support. All of these units were equipped with mechanisms that facilitated remote control of the in-vacuum devices.

monochromator with a 1200 line-per-mm grating. A single bright atomic line was focused onto its exit slit. The light passing through the silt (and through insertable filters of known density) was collimated by a 4.6 m focal length, f/10 mirror. The mirror was remotely adjustable from outside the vacuum and so the light could be directed toward the UVCS, which was mounted on a support that could be remotely translated and pivoted. The collimating mirror and the position of UVCS was adjusted so that the line radiation entered through the UVCS instrument aperture and onto its telescope mirrors completely filling the portion of the mirrors that was not covered by UVCS's internal occulter. That 11 mm wide portion of the mirrors, which is the one used for observations at 2.7 solar radii from sun-center, was the only part of the aperture that could be calibrated during the system level calibration. The UVCS radiometric response was measured against secondary photodiode (cesium telluride and aluminum oxide) standards from the National Institute of Standards and Technology (NIST). The NIST photodiodes resided on x-y translation stages located immediately in front of the UVCS and could be inserted anywhere within the collimated beam. The portion of the light striking each of the telescope mirrors was measured by scanning the appropriate photodiode over the portion of the beam illuminating the mirror. The intensity was uniform to within $\pm$ 10 %. The $\approx$1 mm wide exit slit

Table 11.1: Laboratory measured UV radiometric system responsivities. The relative standard uncertainty in the numbers presented is 16 %.

Wavelength /	System Responsivities		
nm	Ly-α channel	O VI channel	redundant Ly-α path
102.6		0.0033	
104.8		0.0030	
116.5	0.0022		
112.6	0.0020		
123.6	0.0021		0.0010
253.7**	$< 3\times10^{-9}$		

** With instrument configured to detect H I 121.6 nm.

of the predisperser was imaged onto each UVCS slit by a combination of the collimating mirror and the respective UVCS telescope mirror with demagnification by a factor of six. Each slit could be set large enough to pass the entire light bundle, which was passed on towards the respective grating where it was dispersed and focused onto an XDL detector. The count rates registered on the detectors (adjusted by the filters' densities) were compared directly to the output of the NIST photodiodes, thereby giving the system responsivity. Measurements were made for both UV channels at several wavelengths within their respective ranges.

A total relative standard uncertainty of 16 % for each of the radiometric measurements is computed as a quadature sum of the relative standard uncertainties in the calibration of the reference diode (10 %), the uniformity over the telescope aperture of the incident radiation (10 %), the variation of the incident light intensity during a measurement (5 %), and various miscellaneous uncertainties (5 % total) such as the calibration of the current measuring devices, areas of apertures, etc. The results obtained are reproduced in Table 11.1.

Since the laboratory system calibration could be accomplished at only one aperture, the determination of the behavior of the system responsivity of UVCS as a function of aperture was not carried out until after launch. To support in-flight measurements (presented in Section 11.5 of this paper), a laboratory study of the behavior of the efficiency of the UVCS gratings as a function of illuminated aperture was carried out using replicas made from the same masters as the flight gratings. A description of those measurements is published in *Gardner et al.* [2000]. The results are reproduced in Figure 11.3. Because of schedule constraints during the laboratory testing period, complete measurements of the variations of the instrument's responsivities over the full active areas of the detector systems, i.e., the flatfield-calibrations, could not be made. However, representative portions of the detectors were studied with the plan of confirming and extending the measurements in flight.

The laboratory calibration did not include system level measurements of the O VI channel second order responsivity. Estimates of responsivities at second order have been made using measurements of components and taking into account degradation observed in the detector systems.

Based on measurements of the individual components and/or replicas of the individual components, the responsivity at 104.8 nm should be the product of the reflectivity of

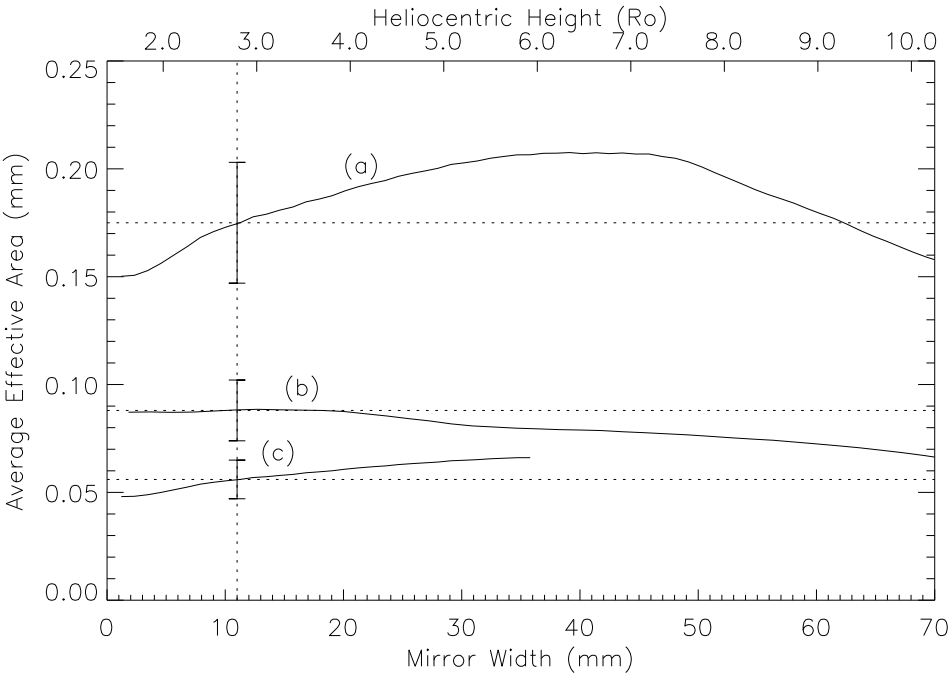

Figure 11.3: Behavior of the UVCS channels as a function of unvignetted width. Curves (a), (b), and (c) show the effective area averaged over the width of the aperture as functions of the mirror width for the O VI Ly-α, and redundant Ly-α channels, respectively, as determined from the laboratory measurements. The error bars denote the standard uncertainty in each curve and are plotted at the launch-locked aperture value of 11 mm. The horizontal dotted lines are provided as an aid to the eye.

the SiC-coated telescope mirror (46 %) [*Osantowski et al.*, 1992], the grating reflectivity (18 %), the groove efficiency averaged over the "standard aperture" of 11 mm width (49 %), and the detected quantum efficiency of the KBr-coated XDL detector (18 %) [*Siegmund*, 1995; *Kohl et al.*, 1995]. However, the product of these numbers is 0.73 %, which is 2.1 times the measured system value. A similar analysis has been carried out for H I Ly-α 121.6 nm, which in the redundant Ly-α path of the O VI channel includes a reflection at an 85 degree angle of incidence (75 % efficient) off the MgF_2/Al coated auxiliary mirror. Here the loss factor is 3.2. Given the nature of the optical components and the environmental conditions experienced by UVCS, we believe the loss in responsivity at both wavelengths is consistent with damage to the KBr coating of the detector from exposure to water vapor (i.e., humidity). A reasonable way to model the loss in responsivity is to take a weighted linear combination of the quantum efficiencies of bare microchannel plates (from the same lot as UVCS) [*Siegmund et al.*, 1995] and of the assumed undegraded KBr coated microchannel plate (i.e., that of the actual UVCS detector) as measured at the component level [*Kohl et al.*, 1995]. It happens that 73 % "bare" plus 27 % KBr provide the observed degradation at both 104.8 and 121.6 nm.

To obtain a responsivity of the UVCS in second order at He I 58.4 nm, we first modify

the efficiency of the XDL detector using the coefficients deduced above and the undegraded efficiencies for 58.4 nm. The overall detector efficiency at 58.4 nm is then reduced from 27 % to 12 %. Multiplying by the component efficiencies at 58.4 nm (telescope mirror, 27 %; average grating efficiency for the first 11 mm, 4.6 %; redundant mirror reflectivity, 70 %) provides a system level responsivity of about 0.10 % for the standard aperture.

An alternative method of estimating the responsivity at 58.4 nm can be made based on the performance of a "life-test" KBr coated detector. *Jelinsky et al.* [1996] report responsivity measurements that have been periodically made for 67 months. The detector, which was stored in dry nitrogen between laboratory air exposures at the time of measurement updates, has shown a 30 % loss of responsivity at 58.4 nm, a 21 % loss at 104.8 nm, and a loss of 36 % at 121.6 nm over the 67 months. Admittedly the environment experienced by the UVCS detectors has been very different from that experienced by the "life-test" unit. Indeed, the latter has likely been better controlled and the environment more benign than that experienced by UVCS during integration and testing. Nevertheless, if one assumes that the UVCS O VI detector has degraded in the same relative proportions as the life-test detector, then the degradation at 58.4 nm can be related to the observed degradations at 104.8 nm and 121.6 nm. Thus, comparing to 104.8 nm, one obtains a degradation given by the ratio of the test detector's degradation at 58.4 nm to that at 104.8 nm (0.30/0.21) times the observed degradation of the UVCS detector at 104.8 nm. The resulting UVCS system level responsivity at 58.4 nm is 0.061 %. Comparing to 121.6 nm, one obtains a degradation given by the ratio of the test detector's degradation at 58.4 nm to that at 121.6 nm (0.30/0.36), times the observed degradation of the UVCS detector at 121.6 nm. The resulting UVCS average system responsivity at 58.4 nm is 0.052 %.

Lacking better information, we choose to algebraically average the three values (0.10 %, 0.061 % and 0.052 %) to obtain a best estimate of 0.071 %. The relative standard uncertainty is estimated to be 50 % of this number. This value reflects the confidence in the methods used and is deliberately chosen to encompass all three values.

11.5 In-flight Radiometric Measurements

In-flight performance has been determined and monitored using specially designed observations of three source types: (1) stars, (2) the solar disk, and (3) the corona at heliocentric heights in the ranges 1.5 to 5.0 $R_\odot$.

11.5.1 Observations of Stars

Observations have been made by UVCS of about 15 stars that pass within 12 $R_\odot$ of sun-center. Voyager, IUE, and FUSE, among others, have made spectral irradiance measurements of one or more of the same stars in spectral ranges overlapping those of UVCS. A typical UVCS measurement consists of a "passage" of the star's image across the UVCS slits. Depending on the details of the trajectory of the star in the sky, the configuration of the UVCS roll and mirror angle can be set such that the angle of the passage relative to the UVCS slit edge is any angle between zero (i.e., perfectly aligned with the long dimension of the slit) and 90 degrees (i.e., at right angles to the long dimension of the slit). The slits are set sufficiently wide and the exposure time is sufficiently short that the entire image

of the star passes through the slits for several exposures. Multiple exposures and multiple passages are summed to improve the statistics for the less bright stars.

Responsivity Changes with Time from Star Observations

The stars that have been observed by UVCS are within its field of view typically for four to five days once per year. Several of the brightest stars have been observed each year of the mission. Some of these observations are suitable for the purpose of monitoring the UVCS radiometric calibration in so far as the stars observed (typically B-stars) have more or less constant emission in the UV. An example of such a set of observations from the O VI channel for the star δ Sco, a binary star system, is presented in Figure 11.4. It has been observed by UVCS with the same or nearly the same instrument configuration in November of every year since SOHO was launched. Figure 11.4(a) shows the spectra observed in 1996, 1999, and 2001. The data were all taken for an approximately 49 mm aperture and therefore are only marginally sensitive to any changes in the responsivity of the first few mm of the mirror. A portion of the spectrum on the left of the figure has contributions from the redundant path. Figure 11.4(b) shows integrals of the spectra from 100 nm to 140 nm (which includes an undetermined portion of "redundant" spectrum) plotted against the year in which each was taken. The data are consistent with a constant behavior of the UVCS radiometric response and the variability of this particular star system within about $\pm$10 %. However the plot suggests a trend toward a lower responsivity, a loss of about 2 % per year. Since the trend could be due to a variation in the UV output of this particular star system, which was observed to produce outbursts in the visible portion of the spectrum during the recent periastron passage [*Miroshnichenko et al.*, 2001], we have examined other data searching for possible response losses, particularly at small apertures.

Like δ Sco, the star ρ Leo has also been observed each year of the mission. The instrument configuration was in general not identical year to year. However, there has been sufficient "overlap" in the observations to provide insight into possible responsivity variations at small apertures. Partial data sets also exist for some other stars as well. In general, there exist a few measurements by other instruments made in this wavelength range for some of these stars. Shown in Figure 11.5 is a plot of the deduced responsivities. Each plotted point is the total count rate observed in a 1 nm band centered on the wavelength noted in the legend divided by the aperture width used for the measurement and then appropriately scaled. The wavelength bands chosen had negligible contributions from the redundant path. The error bars shown are typical of the standard uncertainty in each measurement. The solid black curve is the result of the laboratory component level measurements with the absolute scale set by the laboratory system level calibration at 2.7 $R_\odot$. The 1997 observations of ρ Leo at 101.0 nm were carried out at three apertures. They are normalized to the laboratory curve at the largest aperture and provide confidence that the shape of the laboratory curve is correct for the early part of the mission. In 1996 and 1999 measurements at 106.7 nm of ρ Leo were made at the same aperture of 35 mm. The ρ Leo data from 1999 are actually a series of observations made at a number of different occulter values. The scale of the 1999 data was fixed by assuming a constant irradiance for ρ Leo and using the ratios of count rates observed in 1996 and 1999 for the same aperture. One can readily see that the responsivity at small apertures falls significantly and systematically below the laboratory plot. At the "standard aperture" of 11 mm, the responsivity for

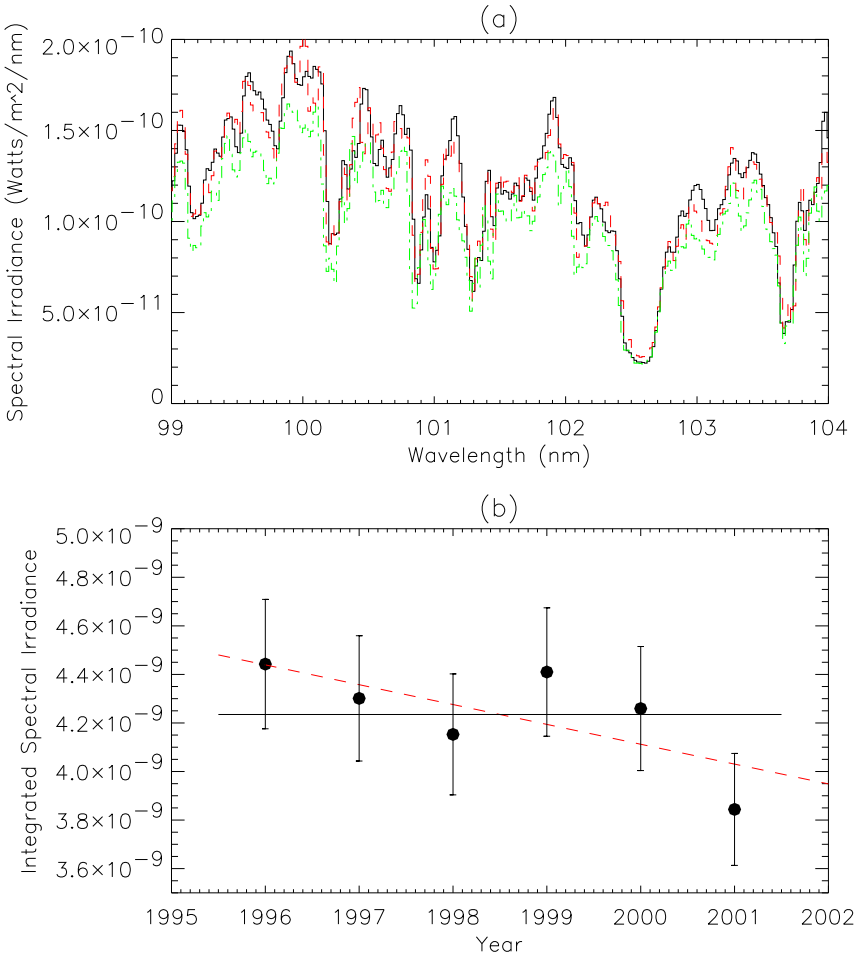

Figure 11.4: Yearly measurements of the short wavelength spectrum of δ Sco. (a) is an over-plot of O VI channel measurements from 1996, 1999, and 2001. The left-most portion of the measured spectrum, in each case, has redundant path contributions. (b) shows a time history of the integral of each measured spectrum from 100 nm to 104 nm. The measurements are constant within 10 %. However, the best fit to the data is a line with a small decreasing trend of 2 % per year. The error bars represent the standard uncertainties including those attributable to the flatfields.

August of 1999 is 80 % of the laboratory value.

In December of 1999 observations were made of θ Oph at 111.1 nm as a function of the aperture. They are also shown in Figure 11.5. UVCS observations do not exist for θ Oph in 1996 or 1997, and consequently the scale cannot be set in the same way as it was for ρ Leo. However the data in 1999 include observations made at relatively large apertures. From the δ Sco observations (see Figure 11.4) it was concluded that for large apertures there is no more than about 6 % degradation from November 1996, until November 1999.

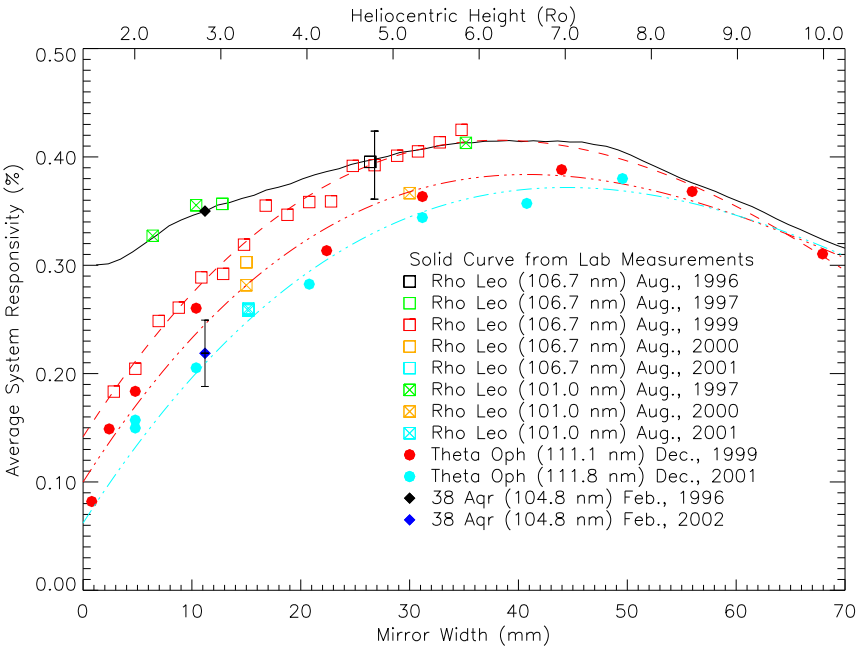

Figure 11.5: Aperture averaged measurements of the system responsivity determined from observations of stars. The identification of the various points is noted in the legend on the plot. The data from 1996 and 1997 are normalized to the laboratory values, which have the same relative variation with mirror width. The later data are put on a common scale through ratios of count rates observed at the same aperture values and the same wavelength for the same star. To connect different stars and thereby extend trends into later years, the relative scales are established using the demonstrated conclusion that the aperture averaged responsivity at apertures beyond 49 mm has changed very little in time. Implicit is the assumption that the irradiances of the stars are nearly constant in time. The smooth color curves, red-dashed, red-dash-dot, and blue-dash-dot, are third degree polynomial fits to the 1999 ρ Leo, 1999 θ Oph, and 2001 θ Oph data, respectively. All three fits are constrained by the two highest aperture points of the 1999 θ Oph data set.

The scale of the 1999 θ Oph data point at 44 mm aperture has therefore been adjusted to 6 % below the laboratory curve. The values at smaller apertures follow the same shape as the 1999 ρ Leo curve within the uncertainties. The values at larger apertures follow the laboratory curve quite well.

In December of 2001 additional aperture scan observations were made of θ Oph at 111.8 nm. Although the data for the two years were taken at slightly different grating angles, they can be accurately put on the same scale, assuming the irradiance of the star is constant in time, using the data at the common apertures of 4.80 mm and 10.39 mm. At such small apertures the part of the spectrum containing redundant path contributions becomes less. One can then compare the data sets at the slightly different wavelength of 110.2 nm, thereby obtaining ratios of 0.82 and 0.79 at the apertures of 4.80 mm and 10.39 mm, respectively. The 2001 scan has been plotted at 80 % of the scale of the 1999

data. Note that the 2001 point at a 49 mm aperture falls very near the laboratory curve. Note also that measurement in 2001 of ρ Leo at a 15 mm aperture, which is scaled to a corresponding 1996 measurement, falls on a smooth interpolation between points on the 2001 θ Oph scan.

There exists one other small set of data that ties recent behavior of the responsivity at small apertures to much earlier times. That data comes from observations of 38 Aquarii, a rather dim star in relation to the ones discussed above. The first measurements took place in February 1996, with an aperture of 11 mm. In February 2001, and again in February 2002, observations were repeated with the same instrument configuration as in 1996. The count rates observed in 2001 and 2002 have the same numerical value. The standard uncertainty is at the 10 % level. When the 1996 datum is normalized to the laboratory value, the 2002 point falls almost exactly on the December 2001, θ Oph curve.

In summary, it is clear that the UVCS O VI channel *has* lost responsivity over the mission. The loss is limited to the the part of the aperture used for observations at low heliocentric heights. The loss is greatest at the edge and tends to become less as the aperture is opened. The data are consistent with the yearly trend noted for large apertures in the δ Sco observations. The data are insufficiently accurate to determine exactly when the degradation began to occur, although there is some evidence that the responsivity in 1997 was about the same as in 1996. Clear evidence exists for degradation by August of 1999. The loss rate at the standard aperture of 11 mm is about 7.5 % per year beginning in 1997, i.e, the responsivity is at 62 % of the value at launch in 2002.

Absolute Stellar Spectroradiometry

Spectra of ρ Leo from the Ly-α channel are shown in Figure 11.6 together with spectra observed by IUE in April of 1980 [MAST Multimission Archive at Space Telescope, file SWP08650]. The UVCS measurements were made in August of 1996 at an aperture width of 26 mm. Assuming the Ly-α channel responsivity behavior in time parallels that of the O VI channel, there should be no degradation from the laboratory values. The UVCS data have been averaged so as to match the spectral resolution of the IUE data set. Coronal emission features (e.g., H I Ly-α 121.6 nm and Fe XII 124.2 nm) and straylight in the raw UVCS spectrum have been removed from the UVCS data. The spectral irradiance measured by UVCS is on average about 1.3 times larger than that found by IUE, nominally at the edge of one standard uncertainty of the comparison. ρ Leo has also been observed by SUMER [*Lemaire*, 2002]. Intercomparisons of UVCS and SUMER using those observations as well as observations of the star α Leo are in process at this writing.

A comparison of UVCS O VI channel observations of the star τ Tau to observations by Voyager [*Holberg et al.*, 1982; *Holberg*, 1992] is presented in Figure 11.7. The measurement was made in June, 2001, at a UVCS mirror aperture of 35 mm. The UVCS responsivity has been adjusted downward by 10 % in accordance with the curves shown in Figure 11.5. The resolution of the UVCS data has been reduced to match the 1 nm resolution of Voyager. The two spectra match on average to within about 15 %, well within the UVCS uncertainty. UVCS has also observed Feige 110, a white dwarf star that is used as a calibration reference for FUSE [*Moos et al.*, 2000; *Sahnow et al.*, 2000]. The star has very weak UV emission as compared to the "hot" stars mentioned above. The integral of the spectrum between 102.6 nm and 103.7 nm measured by UVCS is less than 15 % below that observed by FUSE. The root mean square combined relative uncertainty is 25 %.

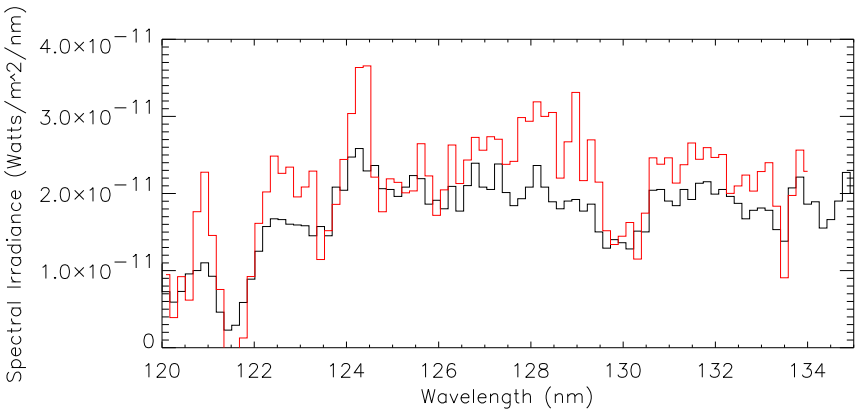

Figure 11.6: UVCS comparison to IUE. The solid dark line is a spectrum taken by IUE of the star ρ Leo. The red line is the UVCS observation of the same star. Coronal emission lines have been removed from the UVCS data. The UVCS data have been averaged to match the 0.17 nm resolution of this particular IUE data set.

UVCS observations of ζ Tau, a hot super-giant star, have been used to develop a technique for separating the overlapping "redundant" (long wavelength) spectrum from the direct (short wavelength) spectrum in the UVCS O VI channel. A paper that describes the details of the method is in preparation [*Valcu*, 2002].

11.5.2 Disk Observations

The first UVCS disk observations were carried out on 31 March 1996. Measurements of the Ly-α radiance were made at a number of positions on the disk in both the Ly-α and O VI channels. Only the first 0.8 mm of the telescope mirrors have ever been exposed to direct disk light. The UVCS neutral density filters, which attenuate Ly-α by a factor of $\approx$ 1000, were inserted to prevent saturation of the detectors.

Inter-calibration with SUMER has been carried out using co-registered and nearly simultaneous observations with both instruments of the N V line at 123.7 nm in 1996 and 1997. These observations were conducted as part of the SOHO Inter-Calibration (ICAL_01) Joint Observation Plan. The data from both instruments are listed in Table 11.2. The UVCS values are on average 18 % lower than those of SUMER. The relative standard uncertainties are 25 % (including counting statistics) in the UVCS values, and a similar value for SUMER. The combined relative uncertainty is thus 35 %, and all of the six data points are inside this value. All of the observations were carried out in 1996 and 1997, and no time related trend to the differences is evident.

11.5.3 Coronal Observations

UVCS Independent Observations

One of the early tasks in-flight was the determination of the UVCS system responsivity as a function of unvignetted aperture (i.e., internal occulter location). The behavior of the

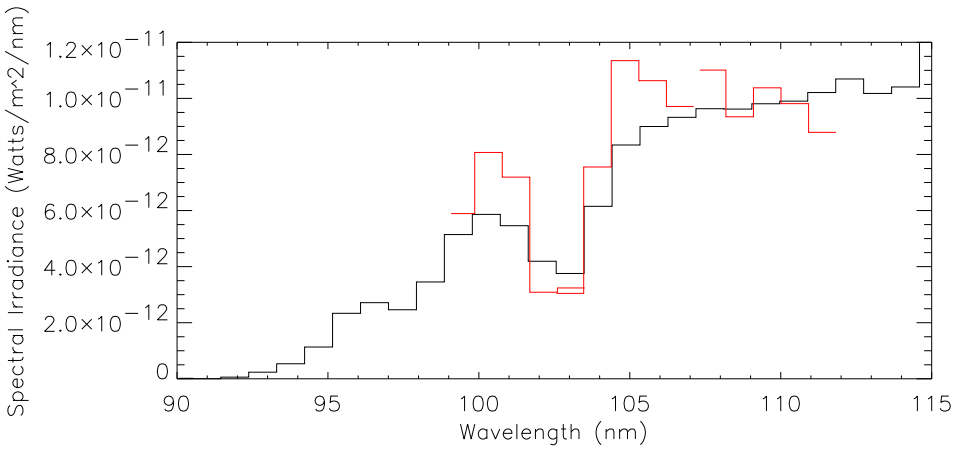

Figure 11.7: UVCS comparison to Voyager. The dark solid line is a spectrum taken by Voyager 1 of the star τ Tau in August 1992. The red line is the UVCS observation of the same star in June 2001. The UVCS data have been averaged to match the 1 nm resolution of Voyager and adjusted to reflect an 8 % loss of responsivity at the 35 mm aperture used for the observation. See Figure 11.5.

primary Ly-α and O VI channels is relatively straight forward to determine; that of the redundant Ly-α path is not. The first such measurements were carried out in March of 1996. The telescopes were pointed to a height of about 2.5 $R_\odot$ in a coronal streamer. Observations of the H I Ly-α line and the O VI lines were then measured in all channels as the occulter was progressively changed from about 9 mm to zero width. The relative changes in intensity are consistent with the laboratory results from the replica grating discussed in Section 11.4.

At heliocentric heights above approximately 6 $R_\odot$ the light detected by UVCS is dominated by the weak H I Ly-α emission of the interplanetary medium. The interplanetary hydrogen gas is expected to be "cold" gas: i.e., its temperature should be about 8000 K [*Clark et al.*, 1995]. The photon emission is weak, about 3×10^7 s^{-1} cm^{-2} sr^{-1}. We have

Table 11.2: Comparison of UVCS and SUMER from ICAL_01 measurements in 1996 and 1997. Photon radiance given in units of 10^{12} s^{-1} cm^{-2} sr^{-1}.

	photon radiance		
Date	UVCS	SUMER	% Difference
96.09.30	3.64	4.66	–12 %
96.10.07	3.52	3.79	–3.7 %
96.11.04	3.64	5.49	–20 %
97.01.30	3.98	4.37	–4.7 %
97.03.14	3.98	3.78	+2.6 %
97.05.16	3.41	4.82	–17 %

used this emission to characterize the relative behavior of the responsivity as a function of aperture at large apertures for both the primary Ly-α channel and the redundant Ly-α path in the O VI channel.

The effective area of the redundant path in the O VI channel is a function of both the grating angle and the unvignetted telescope mirror aperture width. This is because the auxiliary mirror in the redundant path can be filled, over-filled, under-filled or completely missed by particular wavelengths depending on the unvignetted telescope aperture and grating angles. Its complete vignetting behavior has been mapped out using combinations of coronal measurements like those mentioned above at different grating angles in combination with the results of ray traces. The behavior, which includes the combination of the actual telescope mirror unvignetted aperture, the laboratory measured grating aperture non-uniformities, and the geometrical effects of the auxiliary mirror, is presented in Figure 11.8. The function has been incorporated into the UVCS Data Analysis Software.

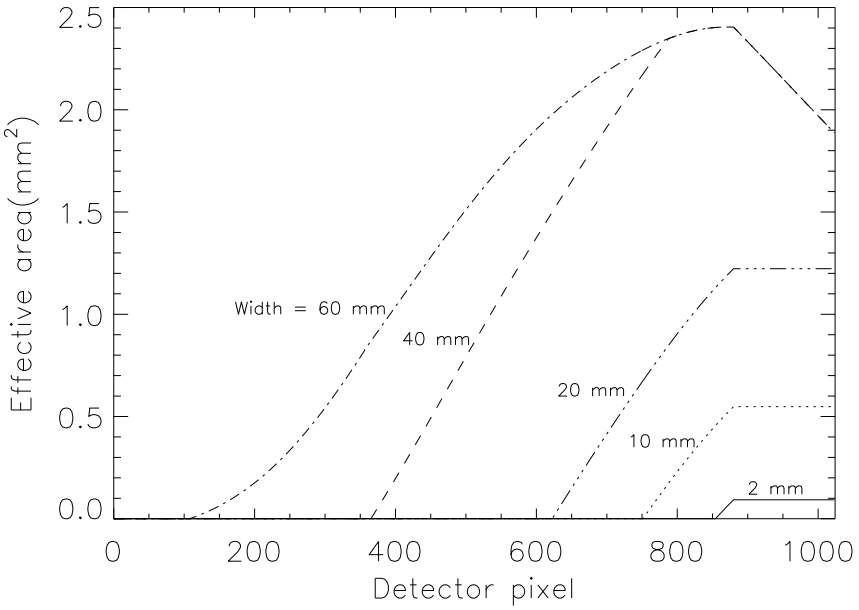

Figure 11.8: Effective area for the redundant path. The effective area is dependent on the actual unvignetted width of the telescope mirror and the vignetting by the redundant path auxiliary mirror. Shown are plots of the effective area for several example mirror widths.

After the recovery of SOHO from its mission interruption in 1998, the coronal aperture scan measurement was repeated with some additions, which allowed an extension of the results to higher aperture. For example, the method was to set the mirror to 3 $R_\odot$, take measurements as the occulter was closed to a position corresponding to about 2 $R_\odot$, then move the mirror to 2.5 $R_\odot$, and continue closing the occulter. Measurements for apertures up to about 4.5 $R_\odot$ were possible in this manner. Above 4.5 $R_\odot$ the emission is too weak to reliably obtain a scan. Such measurements have been repeated several times since the beginning of 2000 as an attempt to monitor changes in the *shape* of the system responsivity function. Since the corona is fundamentally variable, it is difficult to put the scans on a

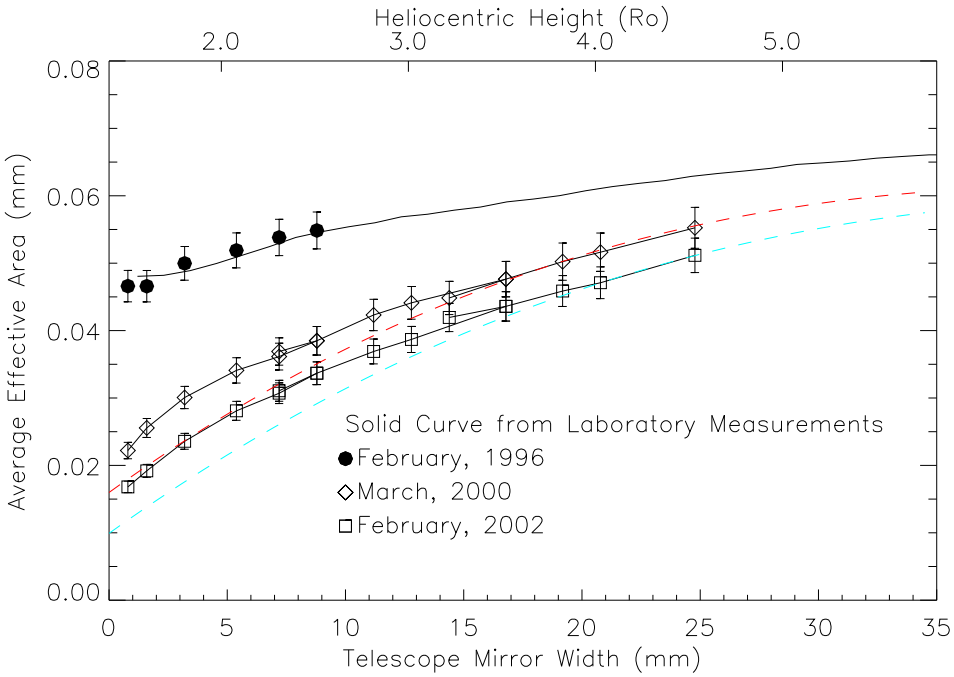

Figure 11.9: Average effective area of the redundant Ly-α path as a function of aperture width setting. Plotted is the maximum average effective area of the redundant path at 121.6 nm for the years 1996, 2000, and 2002. The colored dashed curves are appropriately scaled from Figure 11.5.

common absolute scale. In Figure 11.8 we have normalized the 1996 scan to the laboratory result, and the 1999 and 2002 scans to the corresponding curves obtained from observing stars (see Figure 11.5). The curves indicate a reduction in overall system responsivity of the redundant Ly-α path with time. However it appears that the reduction is less than that for the direct O VI channel. A more definitive conclusion awaits a better normalization for these data.

Intercalibration with Spartan 201

The Spartan 201 spacecraft, a Space Shuttle deployed and retrieved satellite, is comprised of the Ultraviolet Coronal Spectrometer (UVCS/Spartan) and the White Light Coronagraph (WLC/Spartan). UVCS/Spartan views a single spatial element at a time, has less spatial resolution than UVCS/SOHO and observes primarily the Ly-α spectral line. Its basic telescope design is similar to that of UVCS/SOHO. It has made measurements of the solar corona at H I Ly-α on four two-day long flights, the first three occurring in 1993, 1994, and 1995, before SOHO was launched. The last flight occurred on 1 to 3 November 1998, shortly after SOHO was recommissioned after the mission interruption. UVCS/Spartan was radiometrically calibrated in the laboratory before and after each of its flights. Co-temporal and co-spatial observations of H I Ly-α were made in streamers

and coronal holes with both UVCS/Spartan and UVCS/SOHO. After accounting for the responsivity decrease to 75 % of the UVCS/SOHO pre-launch value, the two instruments show agreement within 10 %. If the UVCS/Spartan and UVCS/SOHO calibrations are completely independent, then the uncertainty analysis indicates an expected relative standard uncertainty of 25 %.

11.5.4 Detector Flatfield Measurements

The pixel to pixel variation in the UVCS responsivity has been measured in-flight for large portions of the detectors. The initial measurements and subsequent monitoring utilized a combination of star observations and grating scans. The star observations are used to determine the variations in the direction that is perpendicular to dispersion and grating scans of solar spectral lines are used to determine the variations in the dispersion direction.

The approach for the star observations consists of orienting UVCS and setting each mirror so that a bright star is imaged in the center of each slit's narrow dimension and tracks down its long dimension. Exposures are repeatedly made. The star's spectrum is thus mapped from the "top" to the "bottom" of the detectors. Because of telemetry rate limitations, only a small portion of the spectrum at high resolution can be transmitted to the ground. Four bright UV stars (ζ Tau, α Vir, δ Sco, and θ Oph) have been used in this way. The spatial flatfield calibration can be extended to other portions of the detectors in the spectral direction using grating scans of line radiation (e.g., Ly α) from the corona or disk light diffracted from the external occulter. Additional information about the technique can be found in *Cosmo et al.* [2000].

The procedure is repeated periodically in order to track changes in the detectors' gain with photon dose. The high voltage applied to the microchannel plates is increased to restore the gain before the efficiency of the detector has fallen by more than 5 %.

Flatfield measurements have been made both in the laboratory prior to launch and in-flight. The pixel to pixel variation for the Ly-α detector is $\pm$10 % and the variation for the O VI detector is about $\pm$5 %. Given the magnitude of other uncertainties involved in UVCS radiometry, it is recommended that for essentially all analyses, the user not attempt to correct the data for flatfield variations, but instead adopt the above uncertainties. This is particular appropriate because of the uncertainties introduced by detector degradation as described above. Each detector has a few obvious defects where the detection efficiency approaches zero. Data from such regions should not be used.

11.6 Summary and Conclusions

Pre-flight laboratory measurements were made of the key UVCS/SOHO performance parameters such as spectral resolutions, radiometric responsivities, stray light levels, and flatfield variations over a limited portion of the fields. Measurements made in-flight have, in general, confirmed those laboratory measurements. Because the laboratory system radiometric calibration was only done for one particular limiting aperture (i.e., the one used for observations at 2.7 solar radii), a combination of laboratory component calibrations and in-flight observations were used to extend the calibration to all apertures used during

the mission. Over the six years of operation, the responsivity has decreased in a characterizable fashion for portions of the aperture. The UVCS first order radiometric calibration is in agreement with calibrations of UVCS/Spartan 201, SUMER, IUE, Voyager, and FUSE. Its accuracy is at a relative standard uncertainty of 20 to 22 % depending on the year and the observed height. The second order radiometric calibration of UVCS is based on an analysis of laboratory component calibrations and modeled detector photocathode degradation. It is known only to an estimated relative standard uncertainty of 50 %.

Acknowledgements

This work is supported by NASA under grant NAG-510093 to the Smithsonian Astrophysical Observatory, by the Italian Space Agency, and by the PRODEX programme of ESA (Swiss contribution).

Bibliography

Clarke, J.T., Lallement, R., Bertaux, J.-L., and Quemerais, E., HST/GHRS observations of the interplanetary medium downwind and in the inner solar system, *Astrophys. J.* **448**, 893, 1995.

Cosmo, M. L., Smith, P. L., Atkins, N., Suleiman, R. M., Gardner, L. D., and Kohl, J. L., Flatfield of UVCS detectors for early part of SOHO mission, *Proc. SPIE* **3764**, 161, 1999.

Gardner, L. D., Kohl, J. L., Daigneau, P. S., Dennis, E. F., Fineschi, S., Michels, J., Nystrom, G. U., Panasyuk, A., Raymond, J. C., Reisenfeld, D. J., Smith, P. L., Strachan, L., Suleiman, R., Noci, G. C., Romoli, M., Ciaravella, A., Modigliani, A., Huber, M.C.E., Antonucci, E., Benna, C., Giordano, S., Tondello, G., Nicolosi, P., Naletto, G., Pernechele, C., Spadaro, D., Siegmund, O.H.W., Allegra, A., Carosso, P. A., and Jhabvala, M. D., Stray light, radiometric, and spectral characterization of UVCS/SOHO: laboratory calibration and flight performance, *Proc. SPIE* **2831**, 2, 1996.

Gardner, L.D., Atkins, N., Fineschi, S., Smith, P.L., J.L. Kohl, Maccari, L., and Romoli, M., Efficiency variations of UVCS/SOHO based on laboratory measurements of replica gratings, *Proc. SPIE* **4139**, 362, 2000.

Holberg, J.B., Forrester, W.T., Shemansky, D.E., and Barry, D. C., Voyager absolute far-ultraviolet spectrophotometry of hot stars, *Astrophys. J.* **257**, 656, 1982.

Holberg, J.B., personal communication, 1992.

Huber, M.C.E, Timothy, J.G., Lemaitre, J.S., Tondello, G., Jannitti, E., and Scarin, P., Imaging extreme ultraviolet spectrometer employing a single toric diffraction grating: the initial evaluation, *Appl. Opt.* **27**, 3503, 1988.

Jelinsky, S.R., Siegmund, O.H.W., and Mir, J.A., Progress in soft-X-ray and UV photocathodes, *Proc. SPIE* **2808**, 617, 1996.

Kohl, J.L., Esser, R., Gardner, L.D., Habbal, S., Daigneau, P.S., Dennis, E.F., Nystrom, G.U., Panasyuk, A., Raymond, J.C., Smith, P.L., Strachan, L., van Ballegooijen, A.A., Noci, G., Fineschi, S., Romoli, M., Ciaravella, A., Modigliani, A., Huber, M.C.E., Antonucci, E., Benna, C., Giordano, S., Tondello, G., Nicolosi, P., Naletto, G., Pernechele, C., Spadaro, D., Poletto, G., Livi, S., Geiss, J., Timothy, J.G., Gloeckler, G., Allegra, A., Basile, G., Brusa, R., Wood, B., Siegmund, O.H.W., Fowler, W., Fisher, R., and

Jhabvala, M., The Ultraviolet Coronagraph Spectrometer for the Solar and Heliospheric Observatory, *Solar Physics* **162**, 313, 1995.

Lemaire, P., SUMER stellar observations to monitor responsivity variations, this volume, 2002.

MAST Multimission Archive at Space Telescope, file SWP08650 (ρ Leo).

Mirishnichenko, A.S., Fabregat, J., Bjorkman, K.S., Knauth, D.C., Morrison, N.D., Tarasov, A.E., Reig, P., Negueruela, I., and Blay, P., Spectroscopic observations of the δ Scorpii binary during its recent periastron passage, *Astron. Astrophys.* **377**, 485, 2001.

Moos, H. W., Cash, W. C., Cowie, L. L., Davidsen, A. F., Dupree, A. K., Feldman, P. D., Friedman, S. D., Green, J. C., Green, R. F., Gry, C., Hutchings, J. B., Jenkins, E. B., Linsky, J. L., Malina, R. F., Michalitsianos, A. G., Savage, B. D., Shull, J. M., Siegmund, O. H. W., Snow, T. P., Sonneborn, G., Vidal-Madjar, A., Willis, A. J., Woodgate, B. E., York, D. G., Ake, T. B., Andersson, B.-G., Andrews, J. P., Barkhouser, R. H., Bianchi, L., Blair, W. P., Brownsberger, K. R., Cha, A. N., Chayer, P., Conard, S. J., Fullerton, A. W., Gaines, G. A., Grange, R., Gummin, M. A., Hebrard, G., Kriss, G. A., Kruk, J. W., Mark, D., McCarthy, D. K., Morbey, C. L., Murowinski, R., Murphy, E. M., Oegerle, W. R., Ohl, R. G., Oliveira, C., Osterman, S. N., Sahnow, D. J., Saisse, M., Sembach, K. R., Weaver, H. A., Welsh, B. Y., Wilkinson, E., and Zheng, W., Overview of the Far Ultraviolet Spectroscopic Explorer mission, *Astrophys. J.* **538**, L1, 2000.

Osantowski, J.F., Keski-Kuha, R.A.M., Herzig, H., Toft, A.R., Gum, J.S., and Fleetwood, C.M., Optical coating technology for the EUV, *Adv. Space Res.* **11**, 185, 1991.

Sahnow, D. J., Moos, H. W., Ake, T. B., Andersen, J., Andersson, B.-G., Andre, M., Artis, D., Berman, A. F., Blair, W. P., Brownsberger, K. R., Calvani, H. M., Chayer, P., Conard, S. J., Feldman, P. D., Friedman, S. D., Fullerton, A. W., Gaines, G. A., Gawne, W. C., Green, J. C., Gummin, M. A., Jennings, T. B., Joyce, J. B., Kaiser, M. E., Kruk, J. W., Lindler, D. J., Massa, D., Murphy, E. M., Oegerle, W. R., Ohl, R. G., Roberts, B. A., Romelfanger, M. L., Roth, K. C., Sankrit, R., Sembach, K. R., Shelton, R. L., Siegmund, O. H. W., Silva, C. J., Sonneborn, G., Vaclavik, S. R., Weaver, H. A., and Wilkinson, E., On-orbit performance of the Far Ultraviolet Spectroscopic Explorer satellite, *Astrophys. J.* **538**, L7, 2000.

Siegmund, O.H.W., Stock, J. M., Marsh, D. R., Gummin, M. A., Raffanti, R., Hull, J., Gaines, G. A., Welsh, B.Y., Donakowski, B., Jelinsky, P. N., Sasseen, T., Tom, J. L., Higgins, B., Magoncelli, T., Hamilton, J.W., Battel, S.J., Poland, A.I., Jhabvala, M. D., Sizemore, K., and Shannon, J., Delay-line detectors for the UVCS and SUMER instruments on the SOHO Satellite, *Proc. SPIE* **2280**, 89, 1994.

Siegmund, O.H.W., Gummin, M.A., Sasseen, T., Jelinsky, P., Gaines, G.A., Hull, J., Stock, J.M., Edgar, M., Welsh, B., Jelinsky, S., and Vallerga, J., Microchannel plates for the UVCS and SUMER instruments on the SOHO satellite, *Proc. SPIE* **2518**, 344, 1995.

Siegmund, O.H.W., personal communication, 1995.

Schühle, U., Thomas, R., Kent, B.J., Clette, F., Defise, J.-M., Delaboudinière, J.-P., Fröhlich, C., Gardner, L.D., Hochedez, J.-F., Kohl, J.L., and Moses, J.D., Summary of cleanliness discussion: Where was the SOHO cleanliness programme really effective?, this volume, 2002.

Valcu, B., personal communication, 2002.